Understanding Respiratory Restrictions as a Function of the Scoliotic Spinal Curve in Thoracic Insufficiency Syndrome: A 4D Dynamic MR Imaging Study

Jayaram K. Udupa, PhD, FIEEE, FAIMBE, Yubing Tong, PhD,* Anthony Capraro, MBS,† Joseph M. McDonough, MS,† Oscar H. Mayer, MD,† Suzanne Ho, BA,† Paul Wileyto, PhD,‡ Drew A. Torigian, MD, MA, FSAR, FACR,* and Robert M. Campbell Jr, MD✠†*

Background: Over the past 100 years, many procedures have been developed for correcting restrictive thoracic deformities which cause thoracic insufficiency syndrome. However, none of them have been assessed by a robust metric incorporating thoracic dynamics. In this paper, we investigate the relationship between radiographic spinal curve and lung volumes derived from thoracic dynamic magnetic resonance imaging (dMRI). Our central hypothesis is that different anteroposterior major spinal curve types induce different restrictions on the left and right lungs and their dynamics.
Methods: Retrospectively, we included 25 consecutive patients with thoracic insufficiency syndrome (14 neuromuscular, 7 congenital, 4 other) who underwent vertical expandable prosthetic titanium rib surgery and received preimplantation and postimplantation thoracic dMRI for clinical care. We measured thoracic and lumbar major curves by the Cobb measurement method from anteroposterior radiographs and classified the curves as per Scoliosis Research Society (SRS)-defined curve types. From 4D dMRI images, we derived static volumes and tidal volumes of left and right lung, along with left and right chest wall and left and right diaphragm tidal volumes (excursions), and analyzed their association with curve type and major curve angles.
Results: Thoracic and lumbar major curve angles ranged from 0 to 136 and 0 to 116 degrees, respectively. A dramatic postoperative increase in chest wall and diaphragmatic excursion was seen qualitatively. All components of volume increased postoperatively by up to 533%, with a mean of 70%. As the major curve, main thoracic curve (MTC) was associated with higher tidal volumes (effect size range: 0.7 to 1.0) than thoracolumbar curve (TLC) in preoperative and postoperative situation. Neither MTC nor TLC showed any meaningful correlation between volumes and major curve angles preoperatively or postoperatively. Moderate correlations (0.65) were observed for specific conditions like volumes at end-inspiration or end-expiration.
Conclusions: The relationships between component tidal volumes and the spinal curve type are complex and are beyond intuitive reasoning and guessing. TLC has a much greater influence on restricting chest wall and diaphragm tidal volumes than MTC. Major curve angles are not indicative of passive resting volumes or tidal volumes.
Level of Evidence: Level II—diagnostic.

Key Words: thoracic volume, dynamic MRI, scoliosis, respiratory function, image analysis

(*J Pediatr Orthop* 2018;00:000–000)

From the *Medical Image Processing Group, Department of Radiology; ‡Department of Biostatistics, Epidemiology, and Informatics, University of Pennsylvania; and †Center for Thoracic Insufficiency Syndrome, Children's Hospital of Philadelphia, Philadelphia, PA.
✠Deceased.
Supported by the National Institutes of Health, grant number R21-HL124462 to J.K.U. and R.M.C. The first draft was written by J.K.U. and no honorarium, grant, or other form of payment was given to anyone to produce the manuscript.
The authors declare no conflicts of interest.
Reprints: Jayaram K. Udupa, PhD, FIEEE, FAIMBE, Medical Image Processing Group, Department of Radiology, 3710 Hamilton Walk, 6th Floor, Goddard Building, Rm 602W, Philadelphia, PA 19104. E-mail: jay@mail.med.upenn.edu.

DOI: 10.1097/BPO.0000000000001258

Thoracic insufficiency syndrome (TIS) is a 3-dimensional (3D) deformity of the thoracic components which anatomically and functionally reduces the volume available for ventilation.[1] Over the past 100 years, many orthopaedic procedures have been developed for correcting spine deformity,[2] including spinal fusion,[3] which limits both spine growth and lung function over time.[4] Growth-sparing/growth-promoting methods for spine/chest deformity have been developed, such as growing rods,[5] vertical expandable prosthetic titanium rib (VEPTR),[6] and MAGEC rod.[7] However, none of these methods have been assessed by a robust dynamic metric incorporating thoracic function. The prime measure has remained the angle of the major curve of the spine measured by the Cobb analytic method on radiographic images,[8–10] which has limited health assessment value.[11,12]

Static/dynamic 2-dimensional (2D) slices from computed tomography (CT) and magnetic resonance imaging (MRI),[13,14] static CT-3D,[15] static breath-hold MRI,[16] cine CT,[17] and ultrasonography[18] have been used to define angular and 2D displacements and static lung volumes. However, no attempt has been made to derive 4D measurements from dynamic (4D) image acquisitions. Although pulmonary function testing[11] can indirectly elucidate gross thoracic function, measurements represent summated entities for the

left and right lungs together, such that separation of the biomechanical deficits for individual thoracic components is impossible. The proposed 4D dynamic MRI (dMRI) approach captures the full spatial (3D) and dynamic (4D) information about the whole thorax at every discrete location within the thorax via MRI. From the image so acquired, by using advanced image processing and analysis techniques, the dynamics of the different component structures of the thorax can be analyzed. Unlike any of the above currently available methods, the 4D dMRI method allows examining the structural and dynamic properties of the individual components of the thorax, such as the left and right chest wall and left and right hemi-diaphragm.

The larger goal of our work is to develop via 4D dMRI tidal-breathing functional assessment metrics for the dynamic components of the TIS thorax which relate directly to clinical decision making. In this paper, we focus on one component of that work, namely, investigating the relationship between different spinal major curve types derived from the anteroposterior (AP) radiograph and 4D lung volumetric measurements derived from dMRI. Our central hypothesis is that different AP major curve types induce different restrictions on the left and right lung.

METHODS

Study Group

In this retrospective study, subjects were pediatric TIS patients with all types of thoracic deformity who were treated over a period of 10 years at the Center for Thoracic Insufficiency Syndrome at The Children's Hospital of Philadelphia (CHOP). All consecutive patients with TIS who underwent growth-sparing surgery with VEPTR, and who received both preimplantation and postimplantation dMRI for their clinical care were included in this analysis. Patients who received surgery before their first dMRI, or who had previous chest/heart surgery were excluded. On the basis of these inclusion and exclusion criteria, 13 male and 12 female subjects with age 5.10 ± 4.21 years (preoperatively) and 6.72 ± 4.21 years (postoperatively) were included in this study, with clinical subtypes as follows: neuromuscular = 14, congenital = 7, and other (syndromic and idiopathic) = 4.

Data Gathered

The following data were acquired from patients as part of their routine clinical care, under a research protocol approved by the CHOP Institutional Review Board: patient demographic information, AP and lateral radiographs, and dMRI data of the full thorax preoperatively close to the date of initial surgery and roughly 1 year after initial surgery. For patients younger than 6 years, clinical thoracic dMRI was performed under tidal-breathing conditions while the patient was sedated under general anesthesia with ventilator support. For older patients (above 6 y or as tolerated), dMRI acquisition did not involve use of anesthesia or ventilator support. The scan protocol was as follows: 3T field strength scanner (Siemens Healthineers, Erlangen, Germany); fast imaging with steady-state precession (True-FISP) gradient recalled echo sequence; TR = 3.82 ms, TE = 1.91 ms, voxel size ~$1 \times 1 \times 5$ mm^3, 5 to 10 timepoints over the breathing cycle, $320 \times 320 \times 38$ matrix; acquisition time = 10 to 15 minutes. For each sagittal location through the thorax, slice data were gathered over several tidal-breathing cycles at about 200 ms per slice. The number of 2D slices acquired in this manner is typically 2000 to 3000.

Image Analysis

We derived several key parameters from the dMRI studies using the following 5 steps employing the CAVASS software.[19]

Spinal Radiographic Measurements and Major Curve Type

Thoracic and lumbar major curve angles (denoted TCA and LCA, respectively) were measured by using the Cobb measurement method by a single observer on AP radiographs. Angles of major curves with apices pointing to the right were taken to be positive, whereas angles of major curves with apices pointing to the left were taken to be negative. The radiologist in our team (D.A.T.) reviewed all radiographs and determined the type of major curve (proximal thoracic, MTC, TLC, or lumbar) in each study following the definitions established by the Scoliosis Research Society (SRS).[20]

4D Image Construction

From the acquired 2000 to 3000 slices, using the algorithms of,[21] we constructed 1 4D image constituting the patient thorax over 1 respiratory cycle, where each respiratory cycle comprises of 5 to 8 respiratory phases, and for each phase, the thorax is represented by 35 to 40 sagittal slices. Thus, a 4D image typically consists of 175 to 320 slices. The accuracy of this method in volume measurement has been shown to be about 97% via dMRI experiments involving a 3D-printed dynamic lung phantom.[21]

Segmentation of Thoracic Components

Although the constructed 4D image consists of 5 to 8 respiratory phases, in this work, we focus on the end-inspiration and end-expiration timepoints of the 4D image and estimate how various volumes change between these timepoints. We first segment left lung and right lung in the 3D images corresponding to these 2 timepoints using the algorithm described in Tong et al study.[22] By finding the difference between the binary segmentations in these 2 timepoints, we are able to derive the left and right chest wall and left and right diaphragm tidal volume (excursion) components from the difference binary images.

Measurement of Volumes

From the segmentations in step 3, we compute the following 10 volumetric parameters: left lung volume separately at end-inspiration and end-expiration (LLVei, LLVee); right lung volume at end-inspiration and end-expiration (RLVei, RLVee); left and right lung tidal volume (tv) defined as change in volume from end-expiration

to end-inspiration: LLtv = LLVei–LLVee, RLtv = RLVei–RLVee; left and right chest wall tv (LCWtv, RCWtv), and left and right diaphragm tv (LDtv, RDtv).

Statistical Analyses

To account for patient size variation and its possible effect on volumes, we normalized all volumes by normative (left+right) lung volumes estimated for the patient age and sex from data available in the literature.[23] As our goal in this paper is to investigate the influence of major curve type on tidal volumes, we gathered all 25 preoperative and 25 postoperative cases into a single pool of 50 data sets. We performed 2 types of analysis: (1) We first categorized our 50 data sets into groups based on the SRS major curve type observed without and with regard to the sidedness (left or right) of the apex of the curve. For each of the 10 volume variables, we then compared the groups in pairs via *t* test to determine how the curve type may have influenced volumes. (2) For each group, we analyzed the association between the signed major curve angles (TCA and LCA) and the volume parameters via Pearson correlation.

RESULTS

Figure 1 displays dMRI slices and 3D renditions at end-inspiration and end-expiration of a patient with

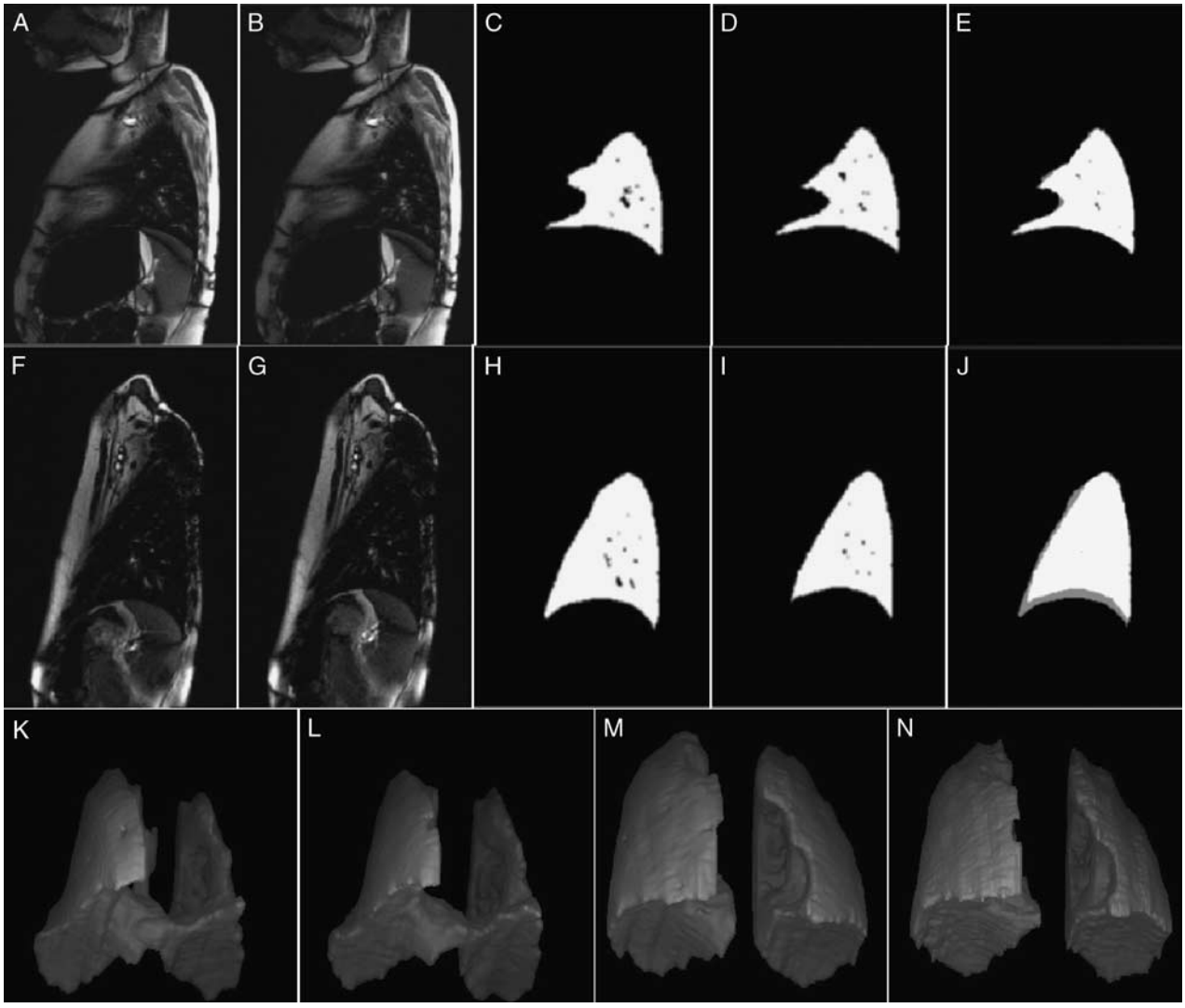

FIGURE 1. Row 1: (A and B) A single representative sagittal True-FISP dMRI slice through right lung from the preoperative 4D constructed image of a thoracic insufficiency syndrome patient in end-inspiration and end-expiration, respectively (all analyses are carried out on full-volume images and not just on slices). C and D, Segmentations of the slices in (A) and (B), respectively. E, The 2 segmentations in (C) and (D) superimposed (where the segmentation for end-inspiration is shown a little darker than that for end-expiration) to show lung motion in the slice plane. Clearly, there is very little motion. Row 2: (F–J) Same as row 1 but from the postoperative dMRI data set of this patient approximately at the same anatomic slice location. Increased chest wall and diaphragmatic motion can be clearly seen. Row 3: 3D renditions of the lungs at end-inspiration (K) and end-expiration (L) for the preoperative condition, and (M, N) similarly for the postoperative condition. Note the relative increase in lung volumes following surgical intervention. dMRI indicates dynamic magnetic resonance imaging.

TABLE 1. Comparison of Thoracic dMRI Volumes Between Major Curve Types Taken in Pairs

Major Curve Types, in Pairs	LLVei	RLVei	LLVee	RLVee	LLtv	RLtv	LCWtv	RCWtv	LDtv	RDtv
MTC vs. TLC	−0.16	−0.40	−0.22	−0.62	+0.72	+0.85	+0.81	+0.85	+0.56	+0.71
	(0.65)	(0.30)	(0.54)	(0.12)	(0.02)	(0.007)	(0.01)	(0.008)	(0.067)	(0.023)
MTC-left vs. MTC-right	+0.32	+0.01	+0.16	−0.13	−0.004	−0.26	+0.17	−0.55	−0.14	+0.06
	(0.46)	(0.99)	(0.71)	(0.75)	(0.99)	(0.52)	(0.68)	(0.17)	(0.72)	(0.89)
MTC-left vs. TLC-left	+0.11	−0.49	−0.12	−0.81	+0.78	+0.58	+0.87	+0.45	+0.56	+0.6
	(0.83)	(0.32)	(0.80)	(0.13)	(0.025)	(0.08)	(0.014)	(0.17)	(0.091)	(0.072)
MTC-right vs. TLC-left	−0.21	−0.45	−0.27	−0.58	+0.85	+0.98	+0.84	+1.01	+0.82	+0.79
	(0.64)	(0.34)	(0.55)	(0.22)	(0.062)	(0.033)	(0.064)	(0.029)	(0.069)	(0.079)

"+" sign for the effect size indicates that the mean volume parameter for the first entity in the pair under comparison is greater than that for the second entity. "−" sign indicates that the mean volume parameter for the first entity in the pair is less than that for the second entity.

The first value in each cell is the effect size and the second value in parenthesis is the *P*-value.

dMRI indicates dynamic magnetic resonance imaging; LCWtv, left chest wall tidal volume; LDtv, left diaphragm tidal volume; LLtv, left lung tidal volume; LLVee, left lung volume at end-expiration; LLVei, left lung volume at end-inspiration; MTC, main thoracic curve; RCWtv, right chest wall tidal volume; RDtv, right diaphragm tidal volume; RLtv, right lung tidal volume; RLVee, right lung volume at end-expiration; RLVei, right lung volume at end-inspiration; TLC, thoracolumbar curve.

neuromuscular scoliosis before (age = 7.4 y) and after (age = 7.9 y) VEPTR surgery. Considerable postoperative increases in chest wall and diaphragmatic excursions can be seen qualitatively from the displays. These increases (in mL) were: LLtv = 49.484, RLtv = 22.027, LCWtv = 24.127, RCWtv = 3.972, LDtv = 25.357, and RDtv = 18.056, with a median and mean value of these increases of 167% and 130%, respectively. Over all patients, the mean and median values of these changes were 70% and 43%, respectively.

In our cohort, SRS-defined curve types for the major curves were as follows: proximal thoracic curve = 5 cases; main thoracic curve (MTC) = 23 cases (with the curve apex to the left for 11 patients and to the right for 12 patients); thoracolumbar curve (TLC) = 11 cases (with the curve apex to the left for 8 patients and to the right for 3 patients), lumbar curve = 7 cases; and other = 4 cases (no curve = 3 cases and not evaluable = 1 case). Because of insufficient number of samples, we performed our analysis on the 23 MTC and 11 TLC cases only. The unsigned major curve angles were: for TCA, min = 0 degree, max = 136 degrees, mean ± SD = 49.9 ± 30.1 degrees; and for LCA, min = 0 degree, max = 116 degrees, mean ± SD = 24 ± 36.5 degrees.

Table 1 summarizes results from *t* testing for comparing volumes between each of 4 pairs of SRS curve types: MTC versus TLC, MTC with curve apex to the left (MTC-left) versus MTC with curve apex to the right (MTC-right), MTC with curve apex to the left (MTC-left) versus TLC with curve apex to the left (TLC-left), and MTC with curve apex to the right (MTC-right) versus TLC with curve apex to the left (TLC-left). The signed effect size and the *P*-value are listed in each cell. A "+" sign indicates that the mean for the first group in the pair is greater than the mean for the second group. A "−" sign indicates that the mean volume parameter for the first entity in the pair is less than that for the second entity. For example, consider the entry in the cell corresponding to column "RDtv" and row "MTC versus TLC." The cell value indicates that the mean value of RDtv for cases when the major curve is the MTC is substantially greater (effect size of 0.71 is generally considered to be large) than the mean value of RDtv for cases when the major curve is the TLC and this difference is statistically significant with a *P*-value of 0.023. This means that the right diaphragm motion is restricted much more by TLC than MTC.

Table 2 lists the Pearson correlations between the volume variables and the signed major curve angles along with the associated *P*-values. For ease of understanding, we will consider 1 example—the only shaded cell in the last column "RDtv." The correlation value of 0.55 suggests that when the major curve is MTC-right, as the LCA increases in magnitude (meaning it becomes more positive), right diaphragm tidal volume increases. This association is moderately strong and its statistical significance is borderline.

DISCUSSION

We make the following observations from Table 1. (i) Row 2: all tidal volumes are higher (with a large effect size) for the MTC cases than for the TLC cases with statistical significance (except for LDtv which shows borderline significance). This implies that TLC has a much higher influence on restricting both chest wall and diaphragm tidal volumes (excursions) than MTC. (ii) Row 3: none of the 10 volume parameters show any statistically significant difference between left-sidedness and right-sidedness of the apex of MTC. (iii) Row 4: LLtv and LCWtv are much higher (large effect size) for MTC-left than for TLC-left, which implies that left-sided TLC restricts LLtv and LCWtv much more than similarly sided MTC. Restrictions on other tidal volumes are similar although these results have borderline statistical significance. (iv) Row 5: even left-sided TLC has much more restrictive influence than right-sided MTC upon right-sided tidal volumes RLtv and RCWtv. This difference in restriction is borderline statistically significant for other tidal volumes.

The data in Table 2 shed light on aspects that are different from those considered in Table 1. (i) When the major curve is MTC or TLC, without considering sidedness, both major curve angles (TCA and LCA) show no meaningful correlation with any of the 10 volume

TABLE 2. Analysis of the Correlation Between Major Curve Angles (TCA and LCA) and Thoracic dMRI Volumes for Different Major Curve Types

Major Curve Type	LLVei	RLVei	LLVee	RLVee	LLtv	RLtv	LCWtv	RCWtv	LDtv	RDtv
MTC (n = 23)										
TCA	−0.04	0.17	−0.02	0.23	−0.05	0.16	−0.11	0.22	0.00	−0.10
	(0.84)	(0.43)	(0.92)	(0.28)	(0.81)	(0.46)	(0.60)	(0.32)	(1.00)	(0.64)
LCA	−0.09	−0.16	−0.01	−0.20	−0.08	−0.17	0.14	−0.18	−0.13	0.06
	(0.70)	(0.46)	(0.97)	(0.35)	(0.72)	(0.44)	(0.87)	(0.40)	(0.54)	(0.54)
TLC (n = 11)										
TCA	−0.05	0.09	0.05	−0.09	−0.32	0.02	−0.08	0.16	−0.43	0.05
	(0.90)	(0.80)	(0.90)	(0.80)	(0.34)	(0.97)	(0.82)	(0.63)	(0.19)	(0.88)
LCA	−0.31	−0.56	0.44	−0.43	0.38	0.00	0.47	−0.17	0.22	−0.07
	(0.36)	(0.07)	(0.18)	(0.19)	(0.25)	(0.99)	(0.14)	(0.62)	(0.51)	(0.84)
MTC-left (n = 11)										
TCA	0.65	0.33	−0.58	0.34	0.46	0.26	0.32	0.45	0.49	0.01
	(0.04)	(0.33)	(0.07)	(0.31)	(0.15)	(0.43)	(0.34)	(0.17)	(0.13)	(0.99)
LCA	−0.50	−0.55	−0.44	−0.55	−0.55	−0.43	−0.42	−0.36	−0.66	−0.38
	(0.12)	(0.08)	(0.18)	(0.08)	(0.08)	(0.19)	(0.20)	(0.27)	(0.03)	(0.25)
MTC-right (n = 12)										
TCA	−0.20	−0.31	−0.17	−0.27	−0.38	−0.41	−0.44	−0.29	−0.45	−0.17
	(0.54)	(0.32)	(0.60)	(0.40)	(0.22)	(0.19)	(0.15)	(0.37)	(0.15)	(0.60)
LCA	0.01	0.11	0.21	0.05	0.44	0.53	0.44	0.34	0.44	0.55
	(0.98)	(0.73)	(0.51)	(0.89)	(0.15)	(0.07)	(0.15)	(0.28)	(0.15)	(0.06)
TLC-left (n = 8)										
TCA	0.00	−0.24	0.02	−0.14	−0.24	0.07	0.14	0.00	−0.43	0.19
	(1.00)	(0.58)	(0.98)	(0.75)	(0.58)	(0.88)	(0.75)	(1.00)	(0.30)	(0.66)
LCA	−0.56	−0.41	−0.61	−0.66	0.29	−0.05	0.46	−0.02	0.05	−0.34
	(0.16)	(0.31)	(0.12)	(0.09)	(0.48)	(0.93)	(0.25)	(0.98)	(0.93)	(0.41)

The first value in each cell is the correlation and the second in parenthesis is the *P*-value.

dMRI indicates dynamic magnetic resonance imaging; LCA, lumbar major curve angle; LCWtv, left chest wall tidal volume; LDtv, left diaphragm tidal volume; LLtv, left lung tidal volume; LLVee, left lung volume at end-expiration; LLVei, left lung volume at end-inspiration; MTC, main thoracic curve; RCWtv, right chest wall tidal volume; RDtv, right diaphragm tidal volume; RLtv, right lung tidal volume; RLVee, right lung volume at end-expiration; RLVei, right lung volume at end-inspiration; TCA, thoracic major curve angle; TLC, thoracolumbar curve.

parameters. (ii) When the major curve is MTC-left, TCA shows moderately strong positive correlation (0.65) with LLVei. Similarly, when the major curve is MTC-left, LCA shows a similar but negative correlation (−0.66) with LDtv. These are the only correlations observed with statistical significance. The first association implies that when the major curve is MTC with its apex to the left, as the thoracic major curve angle increases in magnitude (meaning it becomes more negative), left lung volume at end-inspiration decreases. In other words, this condition impedes left lung expansion during inhalation. The second association suggests that when the major curve is MTC with its apex to the left, as the LCA increases (meaning it becomes more positive), left diaphragm excursion becomes more restricted. (iii) Many moderately strong correlations are observed between major curve angles and volumes (more so with absolute volumes than with tidal volumes) with borderline statistical significance.

To our knowledge, this is the first and only study to investigate how spinal curves impact dynamic thoracic volumetric components in TIS, or moreover in any pediatric ailment. Our study shows how a detailed mapping of the dynamics of the different thoracic components is facilitated by the dMRI method. Such detailed information may be useful to develop knowledge-based and functionally oriented surgery approaches in the future.

Previous studies that investigated the relationship between spinal curve and 3D thoracic geometry have all been carried out in a static manner without involving dynamics. Some of these studies utilized single slice at 1 or multiple vertebral levels and others used full 3D images, mostly from CT. Examples of slice-based analysis are the studies described[24–26] where linear and angular measurements are obtained to study the relative positions of thoracic components and their relationship to major curve angle measured by using the Cobb technique. Static 3D volumetric studies as related to spinal curvature[15,27] are much rarer than the above slice-based studies. Other similar previous analyses differ from our study in 3 fundamental ways: (1) analyses were performed based on 2D or 3D measurements and without the dynamic component captured via imaging, (2) separation of the left and right lung, chest wall, diaphragm components were not performed, and (3) consideration of the curve types were not performed. Because of these differences, it is impossible to relate our results to any existing scientific data.

The main limitation of our study is the small sample size of the patient cohort. This prevented us from making broader observations and more general analysis. This is also the reason that we did not extend our analysis to investigate curve-type–specific differences between preoperatively and postoperative conditions and changes postoperatively. However, as our main goal was to understand how AP spinal curves influence dynamics, overall we had a respectable number of samples—50 dynamic lungs. It is possible that if more samples were available, some of the borderline significances observed in Tables 1 and 2 may turn out to be significant ones. As to power analysis, we did not do any such analysis as we are not interested in estimating sample size requirements for testing specific clinical hypotheses. This is a first study and hence many variables needed for power analysis are unknown at this time. Also recall that some of the patients were on mechanical ventilation support while performing dMRI. While this may have influenced results somewhat, we do not believe that the relationship between spinal major curve type and tidal volumes would have changed significantly due to assisted ventilation. Another potential limitation is that we restricted our analysis to spinal curve information as commonly derived from AP radiographs following current practice. Analysis based on thoracic kyphotic and lumbar lordotic angles derived from lateral radiographs may shed further light on the impact of spinal curves on lung dynamics. Perhaps the spinal curve should be analyzed in a true 3D manner instead of 2D frontal and lateral projections. These are some of the future research directions we intend to pursue in this clinical domain.

CONCLUSIONS

On the basis of thoracic dMRI and image analysis, we showed a unique approach to study lung dynamics in patients with TIS and to relate thoracic dynamics to SRS-defined major spinal curve observable on AP radiographs. Our main conclusions are 3-fold. (i) The relationship between various component tidal volumes and the major spinal curve type is quite complex. In our opinion, this relationship is beyond the purview of intuitive reasoning and guesswork. (ii) As the major curve, TLC has a much greater influence on restricting chest wall and diaphragm components of tidal volumes than MTC. This seems to be true even when the apex of TLC is contralateral to the apex of MTC. The sidedness of MTC as a major curve does not seem to affect tidal volumes in an asymmetric manner. (iii) Disregarding sidedness, neither MTC nor TLC as a major curve shows any meaningful correlation between volumes/tidal volumes and major curve angles. However, moderate correlations seem to exist for specific conditions like left/right lung volumes at end-inspiration or end-expiration.

REFERENCES

1. Campbell RM Jr, Smith MD. Thoracic insufficiency syndrome and exotic scoliosis. *J Bone Joint Surg Am*. 2007;89A(suppl 1):108–122.
2. Weiss HR, Goodall D. The treatment of adolescent idiopathic scoliosis according to present evidence. A systematic review. *Eur J Phys Rehabil Med*. 2008;44:177–193.
3. Stenning M, Nelson I. Recent advances in the treatment of scoliosis in children. *Br Ed Soc Bone Joint Surg*. 2011;1–4.
4. Karol LA, Johnston C, Mladenov K, et al. Pulmonary function following early thoracic fusion in non-neuromuscular scoliosis. *J Bone Joint Surg Am*. 2008;90:1272–1281.
5. Thompson GH, Akbarnia B, Campbell RM. Growing rods in early onset scoliosis. *J Pediatr Orthop*. 2007;27:354–361.
6. Campbell RM Jr, Smith MD, Hell-Vocke AK. Expansion thoracoplasty: the surgical technique of open-wedge thoracostomy (surgical technique). *J Bone Joint Surg Am*. 2004;86:S51–S64.
7. Akbarnia BA, Yazici M, Thompson GH. *The Growing Spine Management of Spinal Disorders in Young Children*, 2nd ed. New York: Springer; 2016.
8. Stokes IAF, Aronsson DD. Computer-assisted algorithms improve reliability of King classification and Cobb angle measurement of scoliosis. *Spine*. 2006;31:665–670.
9. Zebala LP, Bridwell KH, Baldus C, et al. Minimum 5-year radiographic results of long scoliosis fusion in juvenile spinal muscular atrophy patients: major curve progression after instrumented fusion. *J Pediatr Orthop*. 2011;31:480–488.
10. Larson AN, Fletcher ND, Daniel C, et al. Lumbar curve is stable after selective thoracic fusion for adolescent idiopathic scoliosis: a 20-year follow-up. *Spine*. 2012;37:833–839.
11. Mayer O, Redding G. Early changes in pulmonary function after vertical expandable prosthetic titanium rib insertion in children with thoracic insufficiency syndrome. *J Pediatr Orthop*. 2009;29:35–38.
12. Goldberg CJ, Gillic I, Connaughton O, et al. Respiratory function and cosmesis at maturity in infantile-onset scoliosis. *Spine*. 2003;28:2397–2406.
13. Izatt MT, Adam CJ, Verzin EJ, et al. CT and radiographic analysis of sagittal profile changes following thoracoscopic anterior scoliosis surgery. *Scoliosis*. 2012;7:15.
14. Kotani T, Minami S, Takahashi K, et al. An analysis of chest wall and diaphragm motions in patients with idiopathic scoliosis using dynamic breathing MRI. *Spine*. 2004;29:298–302.
15. Adam CJ, Cargill SC, Askin GN. Computed tomography-based volumetric reconstruction of the pulmonary system in scoliosis: trends in lung volume and lung volume asymmetry with spinal curve severity. *J Pediatr Orthop*. 2007;27:677–681.
16. Chu WCW, Ng BKW, Li AM, et al. Dynamic magnetic resonance imaging in assessing lung function in adolescent idiopathic scoliosis: a pilot study of before and after posterior spinal fusion. *J Orthop Surg Res*. 2007;2-20:1–7.
17. Yang O, Lu W, Low DA, et al. 4D-CT motion estimation using deformable image registration and respiration motion modeling. *Med Phys*. 2008;35:4577–4590.
18. Chen W, Lou EH, Zhang PQ, et al. Reliability of assessing the coronal curvature of children with scoliosis by using ultrasound images. *J Child Orthop*. 2013;7:521–529.
19. Grevera GJ, Udupa JK, Odhner D, et al. CAVASS: a computer-assisted visualization and analysis software system. *J Digit Imaging*. 2007;20(suppl 1):101–118.
20. Scoliosis Research Society. Revised glossary of terms. Available at: www.srs.org/professionals/online-education-and-resources/glossary/revised-glossary-of-terms.
21. Tong Y, Udupa JK, Ciesielski KC, et al. Retrospective 4D MR image construction from free breathing slice acquisitions: a novel graph-based approach. *Med Image Anal*. 2017;35:345–359.
22. Tong Y, Udupa JK, Odhner D, et al. Interactive iterative relative fuzzy connectedness lung segmentation on thoracic 4D dynamic MR images, Proceedings of SPIE, 10137: 1013723-1—1013723-6. 2017. Doi:10.1117/12.2254968.
23. Gollogly S, Smith JT, White SK, et al. The volume of lung parenchyma as a function of age: a review of 1050 normal CT scans of the chest with three-dimensional volumetric reconstruction of the pulmonary system. *Spine*. 2004;29:2061–2066.

24. Carlson BB, Burton DC, Asher MA. Comparison of trunk and spine deformity in adolescent idiopathic scoliosis. *Scoliosis*. 2013;8:2. Doi:10.1186/1748-7161-8-2.
25. Newell N, Grant CA, Keenan BE, et al. Quantifying progressive anterior overgrowth in the thoracic vertebrae of adolescent idiopathic scoliosis patients: a sequential magnetic resonance imaging study. *Spine*. 2016;41:E382–E387.
26. Mao SH, Qiu Y, Zhu ZZ, et al. Clinical evaluation of the anterior chest wall deformity in thoracic adolescent idiopathic scoliosis. *Spine*. 2012;37:E540–E548.
27. Wozniczka JK, Ledonio CG, Polly DW Jr, et al. Adolescent idiopathic scoliosis thoracic volume modeling: the effect of surgical correction. *J Pediatr Orthop*. 2016;37: e512–e518.